UNIVERSITY OF GOTHENBURG

Development of a Dosimetric Model for Alpha-Particle Irradiation with ^{213}Bi and an *In Vitro* Experiment to Assess Complex DNA Damage in Human Diploid Fibroblasts

Master of Science Thesis in Radiation Physics

Johnny Kallin

Supervisors

Kecke Elmroth (PhD)

Karin Magnander (MSc)

Jörgen Elgqvist (PhD)

Department of Radiation Physics

University of Gothenburg, 2011

Abstract

Background

The short range and high linear energy transfer of alpha-particles make them suitable for targeting metastatic tumors that have proven difficult to combat using conventional radiotherapy. ^{213}Bi is an alpha emitter with a half-life of 45.59 minutes and can be easily produced using an ^{225}Ac/^{213}Bi-generator, which makes it applicable in a clinical setting.

High-LET radiation causes complex DNA damage, *i.e.* prompt DSBs and clustered lesions. Clustered lesions are defined as two or more lesions within 10 – 20 base pairs of the DNA molecule.

Purpose

The aim was to develop a dosimetric model for alpha-particle irradiation, and to implement it in an *in vitro* experiment using the isotope ^{213}Bi. Further, to assess the amount of complex DNA damage in human diploid fibroblasts following irradiation.

Materials and Methods

The dosimetric model was developed in MatLab and the absorbed dose delivered to cell nuclei was calculated for two alpha-particle energies (8.376/5.869 MeV). Human fibroblasts (HS2429) were cultured in monolayer and irradiated using ^{213}Bi. Postirradiation treatment with base excision repair enzymes Fpg and Nth allowed for cleavage of the DNA molecule at sites of bistranded clustered damages. The amount of prompt DSBs and the amount of newly formed DSBs at clustered damages were quantified using pulsed field gel electrophoresis.

Results

The activity concentration required to deliver an absorbed dose of 25 Gy to cell nuclei was calculated to be 18.48 MBq/cm^3 for an irradiation time of one hour. The dosimetric model was modified slightly and results of the mean absorbed dose were compared to previously published results of mean specific energy within the field of microdosimetry. The amount of clustered damages could not be properly assessed for reasons that are addressed in the *Discussion.* However, the repair of prompt DSBs was examined and discussed in relation to published data and expected radiobiological consequences.

Content

Introduction

Background

Today, conventional external radiotherapy (RT) is used successfully for a wide variety of tumor disease; it is a field that is still in development where advances in techniques such as intensity modulated RT (IMRT) and advanced patient positioning systems push the boundaries of what is treatable. Despite these advances there are types of disease where treatment using external RT will most likely remain non-effective, with widespread metastatic disease probably posing as the best example. However, any tumor that is not well defined or placed in a compromising position presents a challenge to conventional RT. In this problem lies the potential of radioimmunotherapy (RIT) where the general idea is to target antigens specific for tumor cells using antibodies conjugated with radioactive isotopes. This is a field of research that has been actively investigated for more than two decades [1].

The potential for alpha-particle emitters to be applied in therapy has been recognized since the early 1900s [2]. Alpha (α)-particles have a short range (50 – 100 μm) and a high linear energy transfer (LET, ~100 keV/μm) that make them suitable for targeting small volume, and metastatic, tumors with small implications for healthy tissue. Beta (β)-particles have medium range (order of millimeters) and low LET (~1 keV/μm). Their potential for cell killing is thus lower but the range enables a more pronounced crossfire effect which makes them suitable for targeting larger tumors where a portion of the cells might not have the specific antigen targeted [3]. The disadvantage is an increased risk for healthy tissue.

Other advantages of alpha-particles are the dose rate independence and a less pronounced oxygen effect. The dose rate dependence of low-LET radiation can be explained by its sparse ionization pattern. Also, alpha-particles have a higher biological effect compared with low-LET radiation qualities. The relative biologic effectiveness (RBE) is defined as the ratio of the dose from X-rays ($D_{X\text{-}ray}$) to some test radiation (D_r) to achieve the same biological effect (RBE = $D_{X\text{-}rays}/D_r$). It has been shown that the RBE of alpha particles for the induction of double strand breaks (DSBs) in the DNA molecule is larger than unity [4, 5].

A number of alpha- and beta-particle emitters have been investigated as potential candidates for therapeutic use, the vast majority being unusable mainly because of a non-practical half life or a complicated production process. Examples of beta emitters that are used therapeutically are ^{131}I and ^{90}Y and examples of potential alpha emitters that are being investigated are ^{211}At, ^{223}Ra, and ^{213}Bi. In this project the nuclide used for irradiation was ^{213}Bi which mainly is an alpha emitter but also has a beta-decay component. The decay chain also contains gamma components which makes it suitable for imaging bio-distributions. The distribution of ^{213}Bi may also be detected *ex vivo* using the newly developed alpha camera described by Bäck *et al.* [6].

A simplified decay scheme of ^{213}Bi can be seen in Figure 1. The half life of ^{213}Bi is 45.59 minutes and it decays along two branches. It may either decay through beta emission (E_{max} = 1.42 MeV/0.98 MeV) or by the emission of an alpha-particle (5.869 MeV). In 7.4% of the emissions of alphas from ^{213}Bi, the emitted alpha-particle will have a different initial energy (5.549 MeV). Here, all decays have been assumed to result in one 5.869 MeV-particle, which is a reasonable simplification as the total probability of emission of the lower energy alpha-particle is approximately 1.5‰. The resulting daughter nuclei are ^{213}Po and ^{209}Tl. ^{213}Po decays through the emission of an alpha-particle (8.376 MeV) and ^{209}Tl is a beta emitter (E_{max} = 1.827 MeV). Both daughter nuclei decay into ^{209}Pb that, in turn, decays by beta emission (E_{max} = 0.644 MeV). Its half-life is 3.25 h and the final decay product is ^{209}Bi, which is stable [7].

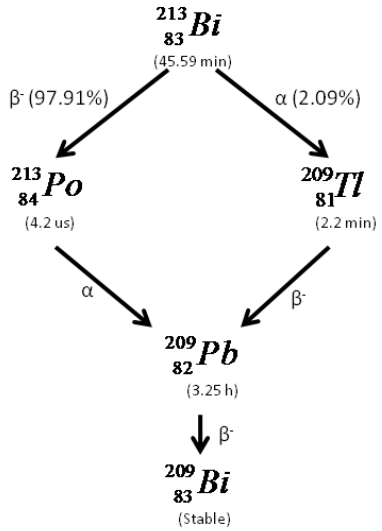

Figure 1. Simplified decay scheme of ^{213}Bi.

The production of ^{213}Bi is made possible by the use of an ^{225}Ac/^{213}Bi-generator. It consists of an ^{225}Ac source dispersed onto a cation-exchange resin from which ^{213}Bi can be eluted [3]. The ^{225}Ac is extracted elsewhere from a mixture of ^{228}Th, ^{229}Th, and ^{232}Th using a four-step chemical process [8]. ^{229}Th is available in increasingly larger supply as it is formed by the decay of ^{233}U which was produced in the US for the *molten salt breeder reactor program* during the 60s and 70s [9]. The generator-protocol is simple, which is a prerequisite for it to be applied clinically. Further details on the elution process of the generator are provided in future sections.

Radiobiology and Clustered DNA Damage

The exact mechanisms by which radiation causes cell death are not completely known but the research is progressing through contributions from many areas within natural science. It is generally accepted that DNA is the main target and the focus of attention has for a long time been on DSBs. However, interest has recently shifted to other complex types of lesions. Examples of less severe damages are single strand breaks (SSBs), oxidized bases or sugars, and loss of bases (AP-sites). See Figure 2 for further details. The induction of two or more of these damages on opposite strands of DNA within one or two helical turns (10-20 base pairs) is what is known as bistranded clustered damages [10, 11]. Though less severe, combinations of these have been shown to be strong contributors to cell lethality [12], and the reason is that the repair mechanisms of complex lesions have been found to be complicated. Not only can lesions in close proximity inhibit repair of neighboring damages, causing persistent mutations or failure in the replication process, but the repair mechanism itself is a source of new DSBs [12]. For example, the repair of an oxidized base by base excision repair (BER) involves removing the damaged base and cleaving the backbone of the DNA in order to replace a section of it. If this damage is complemented by a SSB on the opposite strand, BER could create a *de novo* (new) DSB .

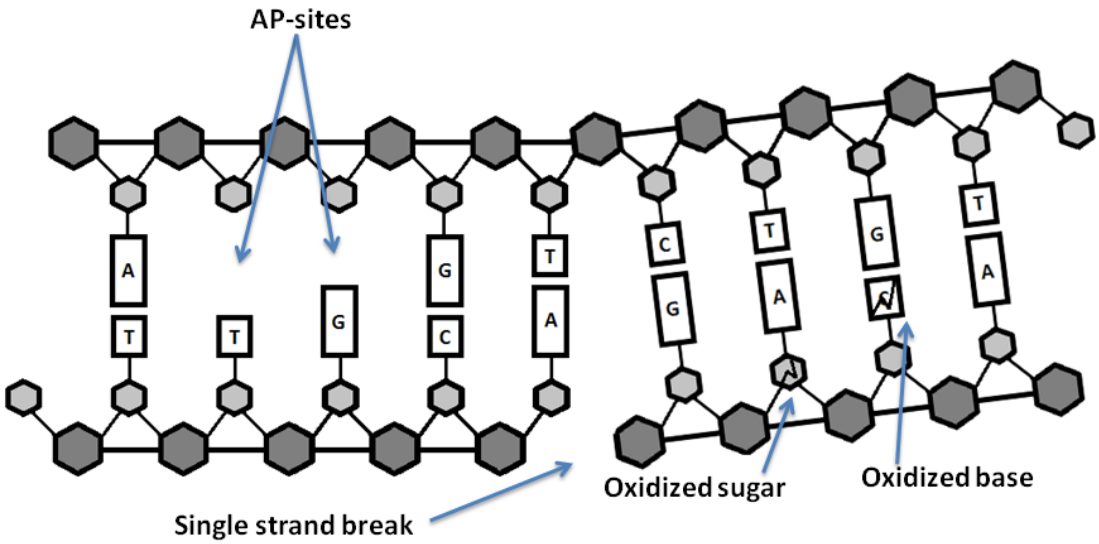

Figure 2. Schematic visualization of clustered damages depicting sites of base loss (AP-sites), single strand breaks as well as oxidized bases and sugars.

To preserve genomic stability several mechanisms for repair have been evolved to counteract various genotoxic effects such as those caused by ionizing radiation. DSBs are mainly repaired by one of two processes, homologous recombination repair (HRR) or non-homologous end joining (NHEJ). HRR can only occur in the S/G_2 phases of the cell cycle and requires contact with an identical patch of DNA which it uses as a template for repair. NHEJ occurs mainly in the G_1 phase of the cell cycle and does not require a template, it simply adds two ends of damaged DNA strands and binds them together in a reaction known as ligation. This process is erroneous by default and may cause a wide variety of chromosome aberrations such as dicentric chromatids or chromosomal rings [13]. If these types of errors are present in mitosis, cells may either die through mitotic catastrophe or be inactivated at later stages of the daughter cells cycles because of the mutations or other forms of chromosomal damage. Another inactivation mechanism is apoptosis which is less common in fibroblasts (the cell type used in this study). Apoptosis, or programmed cell death, is characterized by detachment of the cell from its neighbors followed by condensation of nuclear DNA and subsequent fragmentation of the cell which divides it into a number of membrane-bound apoptotic bodies [13]. It is closely associated with expression of the gene p53 which causes cell cycle arrest in the G_1 phase to allow for DNA repair and to stimulate apoptosis when repair is not possible [14].

There are three main outcomes of faulty repair of DNA damage, the first being that no repair is performed resulting in loss of genetic material. The second is that the repair is incomplete or incorrect which leads to chromosomal aberrations observed after mitosis. The third outcome involves NHEJ and is based on the fact that the ends of a cleaved DNA strand are trimmed off to utilize effective ligation, a process which leads to the loss of genetic material. If the genetic material that is lost contains coding sequences and if the cell does not die as a result of it, it could result in carcinogenesis.

High-LET radiation has been shown to be a source of a larger proportion of complex lesions than low-LET [15]. The ionization density of alpha-particles is high enough so that the distance between ionizations is on the scale to that of the DNA helix (width approx. 2 nm). This means that when an alpha-particle traverses a segment of DNA several ionizations may occur which leads to several damages, the amount depending on the level of chromatin condensation [11]. When analyzing the size distribution of DNA fragments produced by different LET radiations it has been shown that high-LET radiation has a tendency to produce correlated DSBs leading to a larger amount of short

fragments than would be expected from random induction of DSBs, a random induction which is the hallmark of low-LET radiation (*e.g.* X-rays) [16].

Assessment of Clustered DNA Damage

The method to assess the amount of clustered DNA damage chosen for this study is a step-by-step protocol in which naked DNA is extracted by a two-step lysis procedure; the DNA is then subjected to specific enzymes that transform a portion of the bistranded clusters into DSBs by cleavage of the DNA backbone at sites of clustered DNA damage. The formation of DSBs can be viewed as the formation of shorter DNA fragments, and the amount of these fragments formed within specific size intervals can be measured using pulsed field gel electrophoresis (PFGE). PFGE is described further in the *Materials and Methods* section.

In order to detect bistranded clustered lesions they must be isolated from the DSBs formed simultaneously. Figure 3 depicts a schematic description of how the amount of bistranded clustered DNA lesions can be determined. The evaluation of the amount of clustered DNA damages is done by subtracting the number of prompt DSBs as well as the controls and background from the sample that has been irradiated and treated with enzymes that cleave DNA at sites of clustered damage.

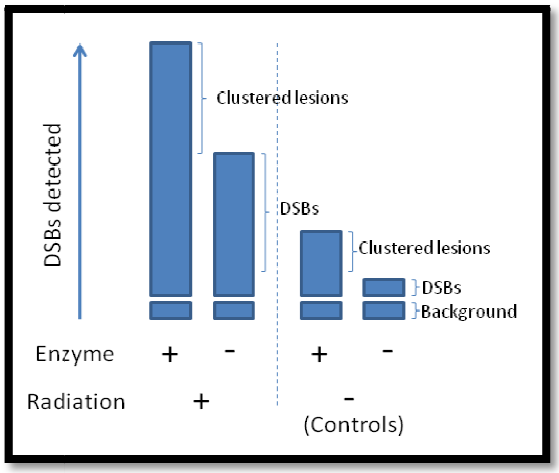

Figure 3. Schematic description of how the amount of clustered lesions can be isolated using PFGE and enzyme treatment of DNA. Inspired by Hada *et al.* [10].

Dosimetry

Regardless of which mechanism causes cell inactivation it is clear that complex DNA damage directly translates to cell death, but the pathways by which this occurs are not perfectly clear and there are confounding factors such as the bystander effect. For clear comparisons to be made between treatments or *in vitro*/*in vivo* trials, where different radiation qualities are used, a clear framework for the dosimetry is needed and there are a large number of methods and protocols described; most widely used perhaps, that developed by the Medical Internal Radiation Dose Committee (MIRD). However, different methods have different limitations and there is still debate as to which approach is the best.

The choice of target plays a major role in the dosimetry of alpha-particles since a single traversal through a cell nucleus has the potential to inactivate a cell. Previously, this was considered definitive, but studies have shown that this number ranges between 1 and 20 traversals [2]. The reason is that a hit does not necessarily imply a large energy deposition. An incident particle could travel straight through the entire diameter of the nucleus but it could just as well graze the surface and even if the particle were to traverse the entire nucleus it would not necessarily traverse DNA, as DNA has the ability to condensate and position itself in clusters. The path length through the nucleus, as well as

the distance travelled prior to entering the nucleus, are important factors that determine the amount of energy deposited. If the particle intersects the nucleus towards the end of its range it could coincide with the Bragg peak as opposed to in an early stage of its path where the stopping power curve is lower and flatter, see Figure 4.

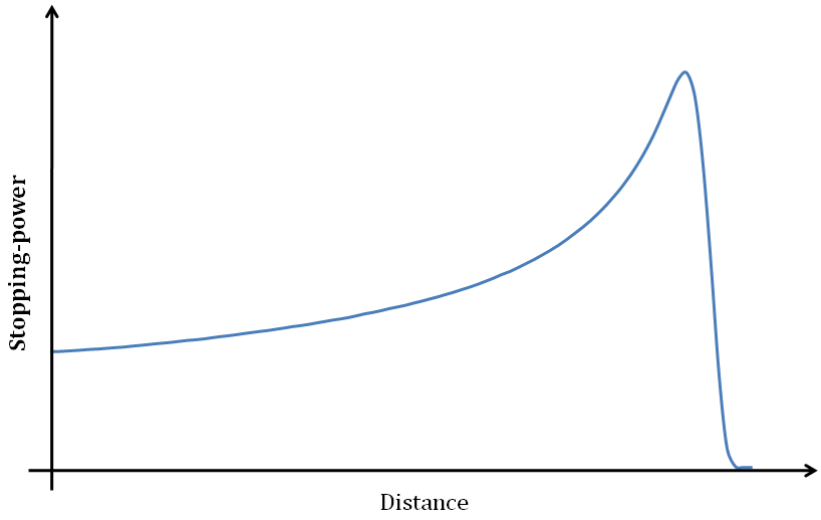

Figure 4. Example of stopping-power curve for an alpha particle with its characteristic Bragg peak.

The stochastic nature of energy deposition is the rationale for microdosimetric approaches and this is considered necessary if the relative standard deviation of the locally deposited dose exceeds 20% [1, 2], which is common when considering small targets such as nuclei of cells. The basic approach in microdosimetry is that both decay position and the direction of emission is determined for an event in a specified geometry; the entry- as well as exit points of particles traversing a target volume are used to determine the path length. The energy deposited within a target volume can be calculated using continuous slowing down approximation (CSDA) range tables or by integration of the stopping-power curve over the distance of interest. There are a number of ways to produce the tables or curves necessary, values provided by the *International Commission on Radiation Units and Measurements* (ICRU) are a common source for stopping-power tables, and Bragg curves can be produced using various Monte-Carlo particle-transport software.

Fundamental quantities in microdosimetry are specific energy (energy imparted per unit mass) and lineal energy (energy imparted per unit path length) and they are often presented in single-event spectra. These are probability distributions of the specific energy deposited in a target for exactly one deposition event (one hit). It is produced by scoring the energy deposition and storing it in a frequency table. The single-event spectrum can be used to determine the multi-event spectrum which is the probability distribution of energy deposition following multiple events (more than one hit). Knowing the single-event spectrum, the multi-event spectrum can be found in several ways; one is to convolve the single event spectrum with itself N-1 times, N being the number of hits [17]. Single- or multi-event spectra can be produced for any source-target geometry using Monte-Carlo software such as Geant4 or MCNPX (support alpha-particle transport simulation) but these are often time consuming and require advanced programming skills on account of the user. There are simpler and quicker models such as the commercial spreadsheet for Excel developed by Roeske [18].

Purpose

The aim of this study was to develop a dosimetric model for alpha-particle irradiation and to implement it in an *in vitro* experiment using the isotope ^{213}Bi. Human diploid fibroblasts cultured in monolayer were irradiated and the goal was to assess the repair of three types of complex DNA damage. The hope was to compare DNA damage with previous trials using ^{211}At and to make

comparisons between the dosimetric model and previously published results by Chouin and Roeske [1, 18] within the field of microdosimetry. Further, a minor experiment to determine the non-specific binding of ^{213}Bi-DTPA to the cell surface was performed.

Materials and Methods

Dosimetric Model

Dosimetric models were developed using MatLab (R2010b, Mathworks) and necessary stopping-power curves were generated using SRIM, a Monte Carlo particle transport simulation software [19]. All written code as well as stopping-power tables can be viewed in Appendix A.

The geometric model was mainly developed to mimic the setting of future *in vitro* experiments and cellular dimensions were based on values presented in a previous master thesis [20]. A visual representation of the geometry can be seen in Figure 5. The target was a circular nucleus with a diameter of 2.5 µm placed at the vertical center of a homogenous cell layer with a thickness of 8 µm. For comparisons to previously published results the geometry was modified and the dimensions and configurations tested are presented in future sections. The density of the nucleus, the cellular layer and the activity solution was set to 1 g/cm^3. ^{213}Bi was assumed to be homogenously distributed throughout a solution covering the cell layer. Two alpha particle energies were considered in this model: 8.376 MeV (97.91%) and 5.87 MeV (2.09%). The alpha particles were assumed to travel in straight lines.

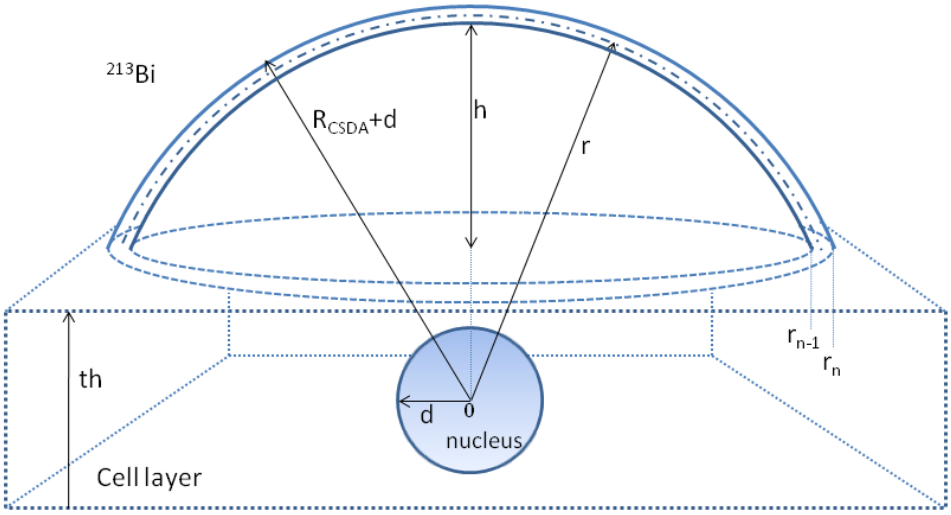

Figure 5. A graphical representation of the geometry used in the dosimetric model. The nucleus with radius d is placed at the vertical centre of a homogenous cell layer with thickness th. The outermost edge of the sphere (contributing to dose) is at a distance R_{CSDA}+d from the origo. The distance to the midpoint of a shell is described by r, the edges of a shell by r_n and r_{n-1}.

Decay was considered if it occurred within a spherical distance R_{CSDA}+d from origo, where R_{CSDA} is the range of the alpha particle according to the CSDA approximation and d is the nuclear radius. The volume of interest (containing activity) was split into concentric shells. The radioactive content of each shell is proportional to its volume which was found using equation (1). *h* is the height from the surface of the cell layer to the edge of a shell and r_n and r_{n-1} designates the edges of each spherical shell.

$$V(r) = \left(\frac{\pi}{3} h_n^{\,2} \left(3r_n - h_n\right)\right) - \left(\frac{\pi}{3} h_{n-1}^{\,2} \left(3r_{n-1} - h_{n-1}\right)\right) \quad (1)$$

The volume of each shell could then be used to calculate the number of decays occurring at each radial distance r by multiplication with the cumulated activity concentration, $\tilde{A}_C(t)$, see equation (2).

$$\tilde{A}_C(t) = \int_0^t A_C(0) e^{-\lambda t} dt \tag{2}$$

The probability of a hit following decay was calculated as the solid angle of the nucleus, from the radial midpoint of each shell, divided by 4π radians, see equation (3). The probability is expected to decrease from a maximum of 0.5 at the surface of the nucleus towards zero at larger distances; this was verified by graphing the probability as a function of distance.

$$P_{hit}(r) = 2\pi \cdot (1 - \cos(\arcsin(d / r))) / 4\pi \tag{3}$$

The dosimetric model was not designed to produce single event spectra but to determine the mean absorbed dose deposited in cellular nuclei. To account for stochastic differences in path length, an approximation was made that the path length of every traversal would equal the mean chord length of the target sphere, 4/3·d, as determined by Cauchy [21], where d is the spherical radius. For each radial distance r, the energy deposition was determined using a Riemann integral evaluated on an interval of a stopping power curve. The interval was based on the nuclear surface as the entry point and the mean chord length as its span. Since the dimensions of the model required higher accuracy than was provided by the stopping-power curves intermediate values were generated by cubic interpolation.

Now, all components necessary to determine the absorbed dose have been presented. The total energy deposition was calculated using equation (4), where $E_{dep}(r)$ is the energy deposition as a function of radial distance and K denotes the total number of shells.

$$E_{tot}(t) = \tilde{A}_C(t) \cdot \sum_{n=1}^{K} V(r_n) \cdot P_{hit}(r_n) \cdot E_{dep}(r_n) \tag{4}$$

The mean absorbed dose was calculated by dividing the total energy deposition with the mass of the cell nucleus and the units transformed from MeV/g to Gy through the multiplication with a constant, see equation (5).

$$D(t) = \frac{1.602 \cdot 10^{-10} \cdot E_{tot}}{4/3 \cdot \pi \cdot d^3 / \rho} \qquad [Gy] \tag{5}$$

For comparisons to previously published results a different approach was adopted. The nucleus was still considered spherical, and the activity was distributed homogenously throughout either the cytoplasm (compartment A) or outside the cell (compartment B). The cell membrane was constructed as concentric around the nucleus, see Figure 6. The energy deposition was found using the Riemann integral evaluated over the mean chord length of the nucleus, as done previously. The volume of the shells in this model was found using equation (6).

$$V_2(r) = \frac{4}{3}\pi(r_n^3 - r_{n-1}^3) \tag{6}$$

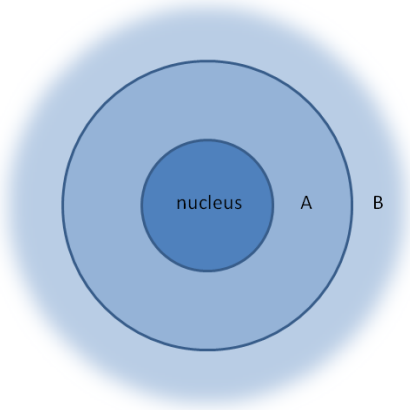

Figure 6. Schematic representation of the geometry used for comparison between the dosimetric model developed here and previously published results. It is constructed of concentric spheres with compartments A (cytoplasm) and B (outside cell) with a spherical nucleus placed at its center.

The published results were based on a Monte-Carlo approach where the radial position of the decay was randomly distributed. To account for an increase in the number of decays at a larger radial distance in the model developed here, the energy deposition vector $E_{dep}(r)$ was weighted using the normalized volume vector V(r), see equation (7). The mean absorbed dose was calculated as before using equation (5).

$$E_{tot} = \frac{\sum E_{dep}(r) \cdot V(r)}{\sum V(r)} \tag{7}$$

SRIM

SRIM is an acronym for *The Stopping and Range of Ions in Matter* and is a group of computer programs that simulate the transport of ions in solids and gases. It has been developed by J.F. Ziegler, M.D. Ziegler and J.P. Biersack and the version used in this study was SRIM v2008.04. The parameters set were initial kinetic energy, target material, number of particles simulated and the particle of choice. The parameter input can be seen in Table 1.

Table 1. List of parameters chosen as input for SRIM, the software used to generate stopping power curves.

Parameter	Input
Initial kinetic energy	8.376/5.869 MeV
Target material	Water (liquid), (density 1 g/cm^3, composition: 66.6% H and 33.3% O, chosen from the compound dictionary)
Number of particles simulated	99,999
Particle	Helium ion (charge +2)

The validity of the stopping power curve was tested by comparison with stopping power curves generated using Geant4 as well as MCNPX, see Figure 7. Results show good agreement with other software. Data was provided through personal communications with Nicolas Chouin (Department of Radiophysics, Gothenburg University), (unpublished data).

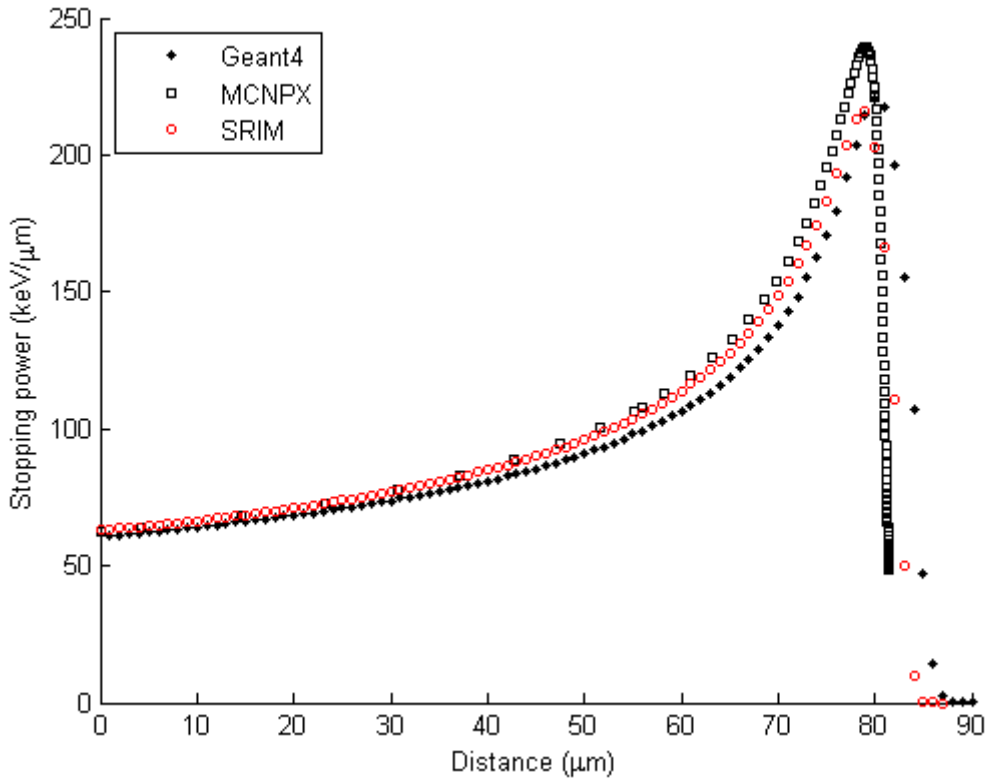

Figure 7. Comparison between stopping power curves for an initial energy of 8.376 MeV generated by different Monte Carlo software. Data was produced in Geant4 (◊), MCNPX (▫) and SRIM (○). Data received through personal communications with Nicolas Chouin (unpublished data).

Cell Cultivation and ^{14}C-Labelling

Normal diploid fibroblasts of human origin, HS 2429 (American Type Culture Collection, Manassas, VA, USA), were cultivated in complete Iscoves medium, with glutamax (Gibco, UK) supplemented with 10% fetal bovine serum (Gibco, UK) and 2% sodium carbonate, in T75 flasks (BD Falcon™) at 37°C and 5% CO_2 in an incubator. To label and distribute cells in T12.5 flasks for use in future irradiation experiments the cell medium was removed and cells were washed with Versene (Gibco, Invitrogen,UK) followed by incubation for a short time period (approx. 2 minutes). The Versene was removed and the cells were suspended (removed from the flask wall) by addition of Trypsin followed by an incubation period of circa 5 minutes. Verification that cells had been suspended was done by visual inspection using a microscope. In cases where a portion of the cells were still attached to the wall the cells were put back in the incubator. New complete medium was added to the suspended cells, with volumes exceeding 10 times that of Trypsin.

Cells were split 1:5 and in order to measure DNA content in the analysis of complex DNA damage cells were labeled with 2 kBq/mL ^{14}C-Thymidine (Amersham Biosciences, UK) which was achieved by adding pre-calculated volumes of [20 kBq/mL] ^{14}C-Thymidine and new complete medium to the cell suspension. This was distributed in T12.5 flasks 5 to 6 days prior to irradiation. Depending on the design of the experiment the number of flasks prepared differed, however, additional flasks were prepared simultaneously to be used for the sole purpose of cell counting.

Irradiation Setup and Protocol

^{213}Bi was eluted from an ITU ^{225}Ac/^{213}Bi-generator (Institute for Transuranium Elements, Karlsruhe, Germany) using a protocol provided by the producer, and labeled with pentetic acid (DTPA). Prior to elution the generator was first rinsed with 3 mL of 0.01 M HCl, the solution was placed in a vial and

pumped through the generator using a peristaltic pump at a velocity of approximately 0.15 mL/min. The resulting eluate was discarded.

For elution, a loading solution (0.3 mL of 0.2 M HCl, 0.3 mL of 0.2 M NaI) was pumped through the generator, extracting ^{213}Bi, and the eluate was deposited in a vial containing the final solution (0.12 mL 4 M sodium acetate buffer, 0.05 mL of freshly made ascorbic acid solution (20%), 0.0067 mL of DTPA (1.5 mg/mL)). The pH of the solution should, according to the protocol, be in the range of 5.3 – 5.5 which was confirmed after the first and one subsequent elution.

After the elution procedure, the generator was rinsed again using 1 mL of 0.01 M HCl and the pump was stopped before the solution had completely passed through the generator, not to let it store dry between elutions.

A volume of 0.73 mL of the eluted ^{213}Bi-solution was transferred to a new vial and placed in a well ionization chamber (Capintec, CRC®15R, Scanflex medical AB) pre-programmed for ^{213}Bi activity measurement. The activity concentration was determined and the solution was diluted using phosphate buffered saline (PBS) to match the activity concentration as calculated by the dosimetric model described above.

Cells were taken from the incubator and placed on ice just before irradiation. At the time of irradiation, 0.8 mL of the diluted ^{213}Bi solution was placed in each cell flask and a timer was set to 1 hour. Irradiation time was adjusted after measuring the activity of 0.8 mL of surplus activity solution some time after the start of irradiation, an additional check to ensure that the dilution had been done correctly. Controls were filled with PBS and all flasks were placed on a rolling board in order for the fluid to wash over the bottom of the flasks.

Flasks were emptied and rinsed 3 times using PBS at the end of the irradiation, controls were rinsed once. After the final rinse in the first trial, a portion of the volume of PBS was placed in an ionization chamber to ensure that no residual activity was still present.

Post-Irradiation Treatment and Lysis Procedure

All post-irradiation treatment was based on protocols used in earlier studies [4, 11]. After irradiation the PBS was replaced by 3 mL of pre-heated pre-gassed complete medium and placed back in incubation to allow for repair. Cells that were not allowed to repair (t = 0) were kept on ice and prepared for lysis. A volume of 0.25 mL of serum free medium was added to these flasks and cells were scraped off the bottom surface. Then, 0.2 mL of the cell suspension was mixed 1:1 with pre-heated Incert agarose (BioWhittaker Molecular Applications, Rockland, MD, USA) in Eppendorf tubes. The agarose/cell suspension solution was placed in moulds on ice and allowed to set; resulting in 4 plugs each with a volume of 85µl.

The plugs were placed in a solution of 0.5 M EDTA with 2% N-laurylsarcosine and 1.4 mg/mL proteinase K as a first step of the lysis procedure known as ESP lysis, with 1.5 mL ESP solution/plug. The plugs were left in ESP for 20-24 hours and the procedure was repeated once a trial's repair incubation time had expired.

After ESP lysis plugs were rinsed with 0,1 M EDTA and left for 1 hour, then transferred to a second solution known as salt lysis (2mM EDTA, 0.5% Triton-X100, 4 mM Tris, 1.85 M NaCl, 0.15 M KCl, 5 mM $MgCl_2$). They were placed in salt lysis for approximately 20 hours and then rinsed using 0.1 M EDTA 2 x 1 hour. At this point the plugs were rinsed with TE buffer (100 mM Tris, 1 mM EDTA, pH 7.5) 6 x 45 min and left in TE buffer over night.

Enzyme Treatment

Of interest in this study were clustered DNA damages and these were evaluated using two separate enzymes, Formamidopyrimidine-DNA glycosylase, Fpg (New England Biolabs, Ipswich, MA, USA) and

Endonuclease (III), Nth (New England Biolabs, USA). These are base excision repair enzymes that remove oxidized bases and cleave the DNA backbone at the damaged site; Fpg targets purines while Nth targets pyrimidines. The addition of enzymes helps transform a portion of clustered damages into DSBs, the amount of which can be determined using pulsed field gel electrophoresis.

In preparation for enzyme treatment Agarose plugs were equilibrated in endonuclease reaction buffer (50 mM Hepes, 125 mM KCl, 0.625 mM EDTA, pH 7.9, 0.25 mg/mL bovine serum albumin) on ice for 1 hour and subsequently placed in fresh endonuclease reaction buffer with or without the enzymes (no enzymes for prompt DSB evaluation, with enzymes for evaluation of clustered lesions). The enzyme concentration was based on the cell count and the desired concentration was $20*10^5$ units/cell/DNA index (DNA index is a measure of the amount of DNA found in cells, for the cell type used here it was considered to be 1). Plugs were left on ice for an additional 30 minutes to allow them to equilibrate with the enzymes and then placed in an incubator at 37°C for 1 hour to start the cleavage process. After 1 hour the plugs were taken from the oven and placed on ice, enzyme activity was halted completely by placing the plugs in cold 0.5 M EDTA. Plugs were rinsed using 0.5 M EDTA 2 x 1 hour.

Pulsed-Field Gel Electrophoresis (PFGE)

Enzymatic treatment produces DSBs and examination of the DNA fragment distribution was done using PFGE protocols. Rinsed plugs were equilibrated in 0,5 x TBE running buffer (45 mM Tris base, 45 mM boric acid and 1 mM Na_2-EDTA) for 1 h prior to insertion into the wells of a gel. Also, DNA length standards were loaded on the gel.

The displacement of DNA fragments in a gel are determined by several factors such as agarose concentration, electric field strength and pulse duration [16]. Two types of PFGE protocols were used, the first optimized to separate DNA fragments in the size interval 1110 – 5750 kilo-base pairs (kbp) with an agarose concentration of 0.8%, field strength 2 V/cm and pulse times increasing in 5 steps from 10 minutes to an hour, resulting in a total runtime of 45 h 40 min. The second protocol for separation of fragments <1110 kbp required a gel with the agarose concentration of 1%, a field strength of 7 V/cm and pulse times increasing in three steps from 10 seconds to 1 minute and 10 seconds; the total runtime was 17 hours 1 minute using far more pulses than the previous protocol.

Gels were stained using an Ethidium Bromide solution (10 mg/mL, Invitrogen) which binds to DNA, and then cut on a UV transillumination table (Mighty Bright, model UVTM-19, Hoefer Scientific instruments, San Francisco, US). The gels were cut at specific positions corresponding to the displacement lengths of standard DNA markers *S. Cerevisiae* (Lonza, Rockland, ME USA), *Lambda* (Lonza, Rockland, ME USA) and *S. Pombe* (Bio-Rad Laboratories, Hercules, CA 94547), see Figure 8 for details. An extra lane was cut in a proximal area of the gel for background measurements.

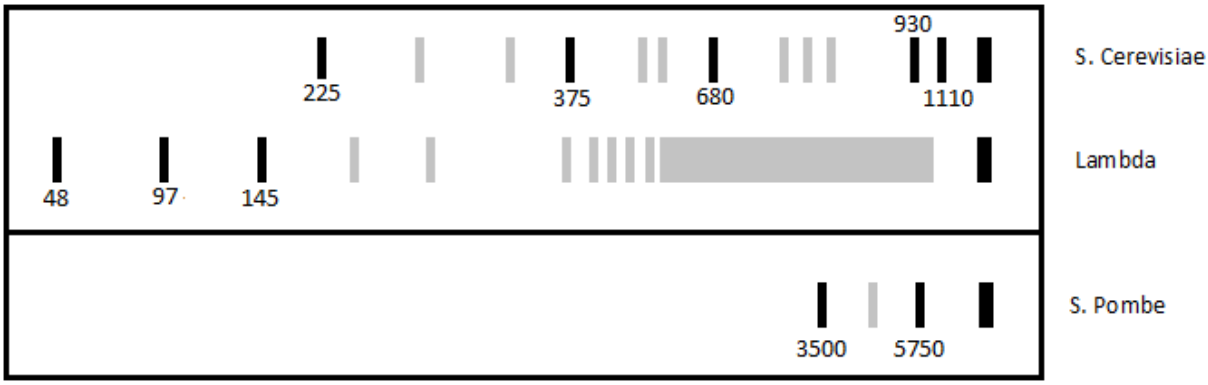

Figure 8. DNA size markers S Cerevisiae, Lambda and S. Pombe. Visualization of DNA displacement following PFGE, sizes in the units of kbp, inspired by Höglund. [16]

The cut out segments of the gel were placed in individual scintillation vials filled with 1 mL of 0.2 M HCl. Distilled water was added to the containers to account for size differences in gel segments, this to counteract geometric differences between individual containers in the scintillation counter. The amount of DNA in each segment was determined by detection of ^{14}C decay (as described previously, ^{14}C-Thymidine was incorporated in the DNA of the cells) in a scintillation counter (Mark II, 4643, Nuclear-Chicago). Each segment was measured twice for the duration of 20 minutes at a preset energy interval.

Data Analysis

Background was subtracted from each sample and the fraction of activity released (FAR) was determined for each size segment and incubation repair time. The total amount of DSBs (n_i) is found by taking the sum of the FAR values (F_i) divided by the mean size of DNA fragments (M_i) in each segment, see equation (8), and do so for all segments. This method is known as fragment analysis.

$$n_i = \sum_i \frac{F_i}{M_i} \tag{8}$$

If the FAR values of each segment are found to be too close to the background it could be necessary to adopt a different method. The level of damage (number of DSBs) is related to the FAR value in a non-linear fashion and is expressed as the number of DSBs per unit length of the DNA [16, 22], see equation (9). $F_{<k}$ is the fraction of activity released (FAR) below some threshold size k, r is the mean number of DSBs per chromosome and n is the average size of a chromosome. This was solved by an iterative process to find the value of r corresponding to the FAR value, including all size segments, for each data point. This method is known as the FAR assay. It is only valid for random induction of DSBs which is not the case with high-LET radiation; this will be addressed in the *Discussion.*

$$F_{<k} = 1 - e^{\frac{-rk}{n}} \left(1 + \frac{rk}{n} \left(1 - \frac{k}{n} \right) \right) \tag{9}$$

Structure and Equilibrium Dose

The structure of the irradiation experiments can be seen in Table 2. Four groups of fibroblast cells were irradiated at different times, and the corresponding repair times studied can be seen in the table. The total number of cell flasks irradiated and studied was thus 13, all accompanied by an equal number of controls.

Table 2. Four groups of fibroblast cell irradiation experiments with corresponding repair times studied.

Repair time / Group	0 hours	40 minutes	2 hours	6 hours	24 hours
Group #1	X	X	X	X	
Group #2	X	X	X	X	
Group #3	X	X	X		
Group #4	X				X

The equilibrium dose presents a method for calculating the absorbed dose in a volume of a solution where charged particle equilibrium is present. This occurs when the energy deposited by a charged particle outside a small sphere surrounding its point of origin is compensated within this sphere by energy depositions made by particles emitted outside the sphere. It is a simple way of quickly calculating the mean absorbed dose in a solution containing a radioactive substance, see equation (10). A_0 is the activity added to the solution at the start of the irradiation, nE is the mean energy per transition and m is the total mass of the active solution.

$$D_{Eq} = \int_0^T \frac{A_0 e^{-\lambda t} nE}{m} \, dt \tag{10}$$

For a geometry where cells are arranged in a monolayer, the dose deposited in a small sphere at the edge of an active solution can be estimated as 50% of the equilibrium dose. This was calculated and compared to the dosimetric model developed for the irradiation experiments with the thickness of the cell layer (depth of the nucleus in tissue) set to zero. The radius of the nucleus was set to 1 µm, which was found to be sufficiently small to accurately estimate the point absorbed dose.

The contribution from beta-particles was roughly estimated using the equilibrium dose, where the mean energy per transition was calculated as one third of the maximum energy of emitted electrons [23]. The transitions considered are those presented in the *Background* section, except for the beta-particles emitted by ^{209}Pb, this will be addressed in the *Discussion.*

Non-Specific Binding

The non-specific binding of the ^{213}Bi-DTPA complex was assessed in a separate experiment. Cells were cultured as in previous experiments and each step of the irradiation procedure was identical as well. The flasks were emptied and rinsed with PBS three times upon completion of the irradiation, and at this point the cells were scraped off the flask wall and a portion of the cell suspension was transferred to vials. All vials were placed in an automatic gamma counter (1480 WIZARD™, Wallac) where the amount of ^{213}Bi decays was measured over a time period of 300 s. The start time of each measurement was noted and used to calculate the residual activity present in the cell layer at the end of the irradiation stage.

Results

Dosimetric Model

The target absorbed dose to the nucleus was 25 Gy (based on previous experiments at the institution using ^{211}At) and the required activity concentration was calculated to be 16.51 MBq/cm^3 for an irradiation time of one hour. This activity concentration was used for the irradiation experiments but was later revised because of a mistake found in the dosimetric model. The activity concentration that should have been used was 18.48 MBq/cm^3 and the lower activity concentration used in the irradiation experiments resulted in an expected absorbed dose of 22.3 Gy, 11% percent below the 25 Gy originally proposed. This will be examined further in the *Discussion*. Comparisons of the mean absorbed dose to published results of mean specific energy can be seen in Table 3 where R_n and R_c specifies the nuclear and cellular radii respectively. The model was applied to different source-target configurations that are visualized in Figure 6. The deviation from results published previously is presented as percentage differences and written in parenthesis (Roeske [18] followed by Chouin [1]).

Table 3. Mean absorbed dose for various source-target configurations and alpha particle energies. R_n and R_c defines the nuclear and cellular radii respectively. The mean absorbed dose is presented in units of Gy. The percentage difference between these values and those of mean specific energy presented by Roeske and Chouin are written in parenthesis (R, C).

	5.87 MeV	8.37 MeV
Cytoplasm (comp. A)		
R_n 4 µm, R_c 5 µm	**0.2673** (14.7, 12.8)	**0.2043** (11.6, 13.5)
R_n 6 µm, R_c 10 µm	**0.1230** (8.8, 8.8)	**0.0922** (7.2, 8.5)
R_n 8 µm, R_c 15 µm	**0.0720** (4.3, 7.5)	**0.0528** (7.8, 7.8)
Outside cell (comp. B)		
R_n 5 µm, R_c 10 µm	**0.2331** (-4.5, -5.6)	**0.2121** (-5.5, -4.5)
R_n 8 µm, R_c 15 µm	**0.0824** (-12.3, -13.3)	**0.0779** (1.2, -1.4)

Equilibrium Dose

Half the equilibrium dose was calculated and compared to the dosimetric model developed for the irradiation experiments. The two values of mean absorbed dose were compared and found to differ by less than 0.4%.

Half the equilibrium dose was used for a rough calculation of the contribution from electrons. It was found that the contribution from electrons was approximately 5%.

Non-Specific Binding

A minor experiment was performed to assess the amount of activity that was not removed by the washes at the end of an irradiation experiment. Counts recorded over 5 minute intervals and the corresponding activity at the time of the washes can be seen in Table 4. The mean activity with the controls subtracted was 208.9 ± 98.5 Bq. The activity that was present just before the washes was calculated and found to be approximately 5.3 MBq.

Table 4. Recorded counts and calculated activity at the time of the washes.

Position	Time after washes (min)	Counts	A_0 (Bq)	Mean (Bq)
1	18.5	38066	168.1	
2	23.7	29123	139.2	209.9
3	28.9	62318	322.4	
4	34.1	179	1.0	
5	39.3	189	1.1	1.0
6	44.5	148	1.0	

The measurement of the PBS solution after the final rinse in the first trial resulted in no notable detection of activity, further emphasizing the apparent effectiveness of clearing the activity with three rinses.

DNA Damage Repair

The purpose of this study was, in part, to assess the repair of complex DNA damage in human diploid fibroblasts irradiated with ^{213}Bi. For reasons that will be addressed in the *Discussion* the target dose of 25 Gy was most likely not achieved which resulted in FAR values that were in level with the background, especially in the PFGE protocol designed to separate fragments smaller than 1110 kbp in length. Because of this an alternate type of data analysis was performed. As described in the *Data analysis* section, the number of DSBs could be determined from FAR values using Blöchers random breakage formula. This was only done for fragments smaller than 5.7 Mbp in the protocol designed to separate fragments in the range 1110-5750 kbp. A curve presenting the fraction of the initial amount of prompt DSBs as a function of repair time can be seen in Figure 9, where the error bars represent the standard error of the mean (SEM).

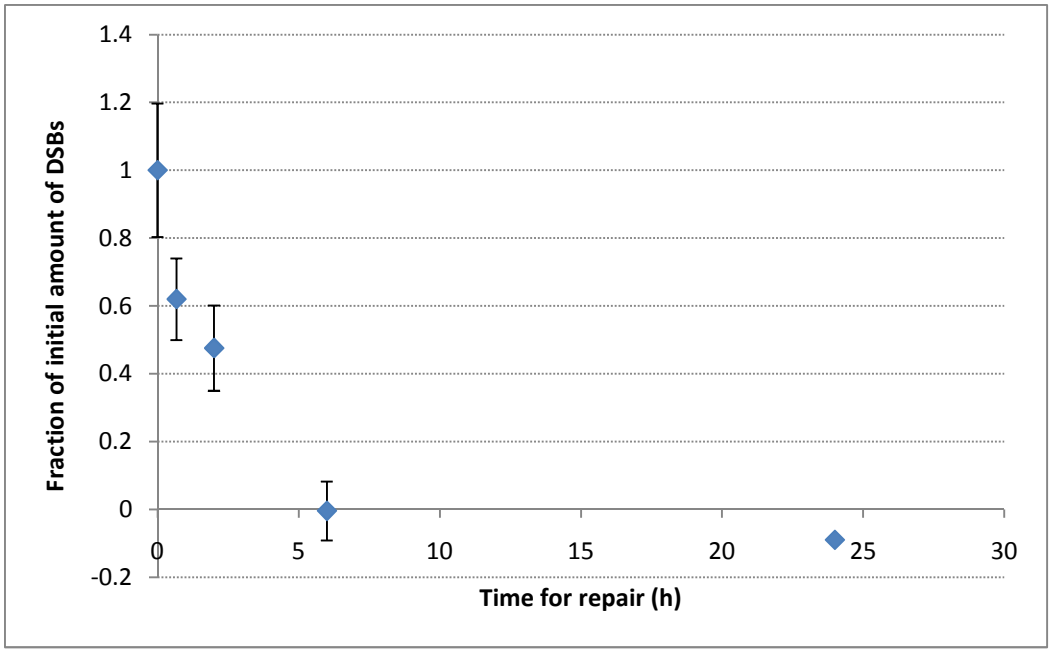

Figure 9. Normalized DSB repair curve as function of time, error bars represent the standard error of the mean. The sample size varied between 1 and 3.

The amount of DSBs quickly decreased in the first 6 hours of repair to a point where it was in level with the controls. The number of DSBs/100 mega base pairs (Mbp) calculated with Blöchers formula for all groups are presented in Figure 10. The bars represent in order from left to right: 1. prompt DSBs. 2. The total number of DSBs present after enzyme treatment with Fpg (both prompt DSBs as well as *de novo* DSBs formed at sites of clustered DNA damage). The total number of DSBs present after enzyme treatment with Nth. The number of clustered DNA damages was not calculated. It would have been found by subtracting the number of prompt DSBs as well as controls and background from the sample that was irradiated and treated with enzymes. The reason for not calculating clustered damages by this subtraction was the occurrence of negative DSB values and that the FAR values were in level with the background as mentioned previously.

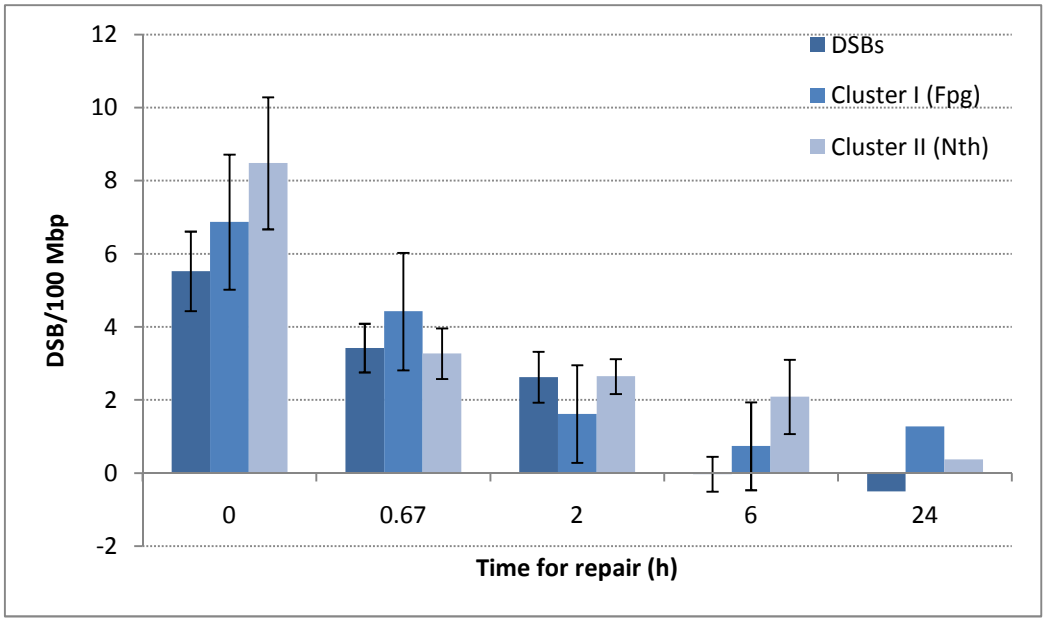

Figure 10. The number of DSBs/100 Mbp for three categories: prompt DSBs, DSBs from Fpg enzyme treatment as well as DSBs from Nth enzyme treatment. Error bars represent the standard error of the mean. The sample size varied between 1 and 3.

Discussion

Two dosimetric models were developed and aspects of the dosimetry have been compared to previously published results. The model was based on a series of assumptions; that alpha particles can be assumed to travel in straight lines, that the mean chord length is a good approximation of the actual mean path length of particles and that the model accurately describes the cellular geometry. There are, of course, uncertainties associated with these assumptions but they have been explored, and if possible, minimized. The impact of variations in the geometry was examined. With variations in the cell layer thickness the predicted dose could increase as much as 5.6% (thickness reduced to 5 µm instead of the suggested 8 µm). Variations in cell nucleus radius had smaller impact with deviations below 1% (cell nucleus radius of 1.5 or 4 µm instead of 2.5 µm). This emphasizes the difficulty in applying a physical model to reality, as there is bound to be natural variations in the geometry of living cells or tissue. Further, it highlights the necessity for clear guidelines regarding the dosimetry for comparisons to be made between studies at different locations.

There was no distinction made between the chemical composition of the cellular structure and the solution containing activity. The density of all components of the geometry was approximated to 1 g/cm^3. Although this most certainly deviates somewhat from the actual density of fibroblasts the question is what impact it had on the absorbed dose. Alpha-particles with initial kinetic energy 8.376 MeV have a range in water of approximately 84.5 µm. There are no stopping power data on fibroblasts per say, but there is data on other tissues such as striated muscle or adipose tissue, and the CSDA range in these deviates from that in water with a few µm; the alpha-particles have a range of cirka 81.4 µm in striated muscle and 86.2 µm in adipose tissue [24]. It is unlikely this would have a significant impact on the absorbed dose since a decrease in the range would be counteracted by an increase in the LET of the particles emanating from the remaining shells and vice versa.

The assumption that alpha-particles travel in straight lines is common in simple microdosimetric models since it enables the particle track to be described using the equation of a straight line. It has been shown to be a valid assumption for alpha-particles with an initial kinetic energy lower than 10 MeV [2]. In addition, the lateral dispersion may be ignored as the width of the alpha particle track is considerably smaller (~100 nm) than the width of the nucleus (diameter > 1 µm) [17].

Only alpha particles were considered in the dosimetric model. The exclusion of beta particles and gamma radiation was done for several reasons. The contribution of gamma particles to the absorbed dose may be considered marginal because of its long range and low ionization density. To accurately calculate the contribution of beta-particles to dose in the specific geometry presented here, a completely separate dosimetric model would have had to be developed. The minute mass of electrons makes them scatter easily and the beta decay produces electrons with a range of energies which further complicates the calculations. One method would be to employ a dose point kernel (DPK) based on Monte Carlo simulations and try to estimate the contribution but this would not include electrons backscattered in the bottom wall of the flasks. In essence, the most reliable method would likely be to simulate the entire geometry using Monte Carlo software.

A rough estimation was made of the contribution to dose from beta-particles using half the equilibrium dose. It was found that the dose from electrons, if charged particle equilibrium could be assumed to exist, would be approximately 5%. The contribution from ^{209}Pb was excluded since its half-life is too large in comparison to ^{213}Bi resulting in a negligible build-up of activity within the time span of a 1 hour irradiation.

The range of beta particles is on the scale of millimeters and appropriately matching the model to the real cellular geometry would have become more challenging as the height of the fluid pillar containing activity is difficult to determine correctly because of capillary forces pushing fluid to the edges of the cell flasks. The height of the pillar was likely less than 0.5 mm and in combination with the fact that the DNA damage potential of beta particles is lower than that of alpha-particles, it can be assumed that the dose would not have increased significantly due to the contribution of beta particles. However, it was a deliberate estimation and as a result of it the dose was certainly somewhat underestimated.

A miscalculation was made in the first dosimetric model which resulted in an incorrect determination of the activity concentration needed to achieve a mean absorbed dose of 25 Gy to the nucleus. It was determined to be 16.51 MBq/cm^3 and later revised to 18.48 MBq/cm^3. According to the revised model an activity concentration of 16.51 MBq/cm^3 would result in an absorbed dose of approximately 22.3 Gy, a decrease of almost 11%. This will be discussed in relation to the results of the irradiation experiments.

Mean absorbed dose for various source-target configurations was compared to previously published results of mean specific energy. An interesting feature of Table 3 is that for the activity distributed in the cytoplasm all values are higher than those published, while the opposite is true for activity distributed outside the cell (with one exception). A possible explanation for the underestimation with activity distributed outside the cell is that the previously published results were based on ICRU tables that do not include extensive range straggling data which would result in a tail on the stopping power curve. The occurrence of such a tail increases the amount of particles that stop within the target and only deposit a small amount of energy, lowering the mean absorbed dose. However, this has not been thoroughly investigated and the actual decrease might be negligible.

The non-specific binding of ^{213}Bi-DTPA to the surfaces of cells was examined and it was found that only a small amount of activity still resided on the cells after three rinses with PBS. The activity of 209.9 Bq was dispersed on the entire surface of the cell monolayer and the contribution to dose can be assumed to have been minimal. The result indicates that three rinses are adequate while it might be sufficient with fewer.

The detection method for DSBs using PFGE has progressed from where DNA fragments could only be separated using a single size threshold, such as the separation of fragments smaller than 5.7 Mbp in length. This method is known as the *FAR assay.* FAR values can be re-calculated into DSBs and the reason for doing so is that FAR does not have a linear response to dose, while it has been proven that

DSBs do. The FAR assay is adequate when DNA breaks are randomly distributed, as is the case with low-LET irradiation. However, this method has proved insufficient when considering high-LET irradiation. The reason is that high-LET radiation produces correlated breaks in close proximity resulting in an increase of small DNA fragments. For example, Löbrich *et al.* [25] irradiated human fibroblasts (GM38) using N and Fe ions with LETs 97 and 150 keV/µm respectively, and found such an increase in the number DSBs using *fragment analysis* capable of separating smaller fragments. Further, Höglund and Stenerlöw [26] showed that N ions with LETs 125 and 225 keV/µm produced a larger proportion of small fragments in human fibroblasts (GM5758) than ^{60}Co photons.

It is expected that complex DNA damage, *e.g.* DSB, induced by high-LET radiation is more difficult to repair than lesions formed after irradiation with sparsely ionizing radiation. The results presented in Figure 9 show a rapid decrease in the number of DSBs. Within 2 hours of repair incubation, approximately 50% of the DSBs were found to have been repaired, and in 6 hours, no DSBs remained. In contrast, Claesson *et al.* [27] found that the fraction of DSBs remaining after 6 hours of repair incubation was approximately 80% after irradiation of stationary human fibroblasts (HS2429) using the alpha-particle emitter ^{211}At (30 Gy). The study employed fragment analysis. Karlsson and Stenerlöw [28] reported that in normal human fibroblasts, irradiated with 125 keV/µm N ions (20 Gy), 20% of the initial amount of DSBs was still present after 4 hours of repair when quantified using PFGE. They also found that 34% of the initial amount of γ-H2AX foci, a molecular marker activated at DSB sites, was still present after 8 hours of repair incubation following irradiation with high-LET particles as compared to 5% in samples irradiated with photons. The quick decrease seen in Figure 9 would have been expected following low-LET irradiation as widely spaced DSBs are repaired quickly. In support of this, Wang *et al.* [29] have presented results suggesting that the occurrence of small fragments inhibit NHEJ since short fragments reduce the possibility for a specific repair signaling enzyme to properly bind at the ends of small fragments. In addition, Claesson *et al.* [27] have found that repair of non-correlated breaks is prioritized even for low-LET irradiation as the non-random component of DSBs increased with repair time.

The reason for the quick repair seen in this study (Figure 9) is likely that the method used was the FAR assay; the smaller fragments that are repaired late are not included. The reason for not including these was that the recorded FAR values for smaller fragments were in level with the background resulting in negative values on a large portion of the fragment sizes examined. The reasons for this are not perfectly clear, but one possible explanation could be that the lysis procedure was incomplete. If the lysis had failed, there would not have been naked DNA residing in the plugs loaded on to the PFGE gel. As large structures (whole cells, nuclei) cannot migrate in the gel the activity would remain in the wells resulting in FAR values in level with the background. This is an unlikely scenario as studies performed simultaneously using the same lysis products showed no such tendencies.

Another source of error could be the scintillation measurements, but activity was recorded in the wells of all gels and it is highly unlikely that the error was present only when measuring the vials containing fragments that had been displaced further in the PFGE gel. If the electrophoresis had been faulty, not only would the DNA fragments from irradiated samples be left in the wells, but this would also be true for the standard DNA length markers. As this was not the case, this hypothesis can also be rejected. The enzymes used to cleave DNA strands at sites of base damage are a possible source of error but the FAR values were low in the prompt DSB group, where no enzymes had been utilized, as well.

The most likely explanation for the low FAR values lies in the irradiation stage of the experiment. Flasks were placed on ice on top of a rolling board with the intention that the active solution would wash over the surface of the cells. Measures were taken to level these to ensure full coverage of the cell monolayer, but even a minor tilt could possibly have shifted the liquid to one corner. And, if the ice melted unevenly during the irradiation it would create the same effect. It seems probable that

most cells have received a dose that was much lower than the 25 Gy proposed which could also be the result of a major fault in the dosimetric model. In revision, no such mistakes have been detected but it cannot be completely ruled out. However, the good agreement of the calculated mean absorbed dose in comparison with the equilibrium dose would further suggest that no major faults are present.

Finally, the correction of the expected mean absorbed dose from 25 Gy to 22.3 Gy as a result of a miscalculation in the dosimetric model would not be sufficient to explain the decrease in the fraction of activity released though the dose is lower than what was originally proposed. The initial amount of DSBs was found to be approximately 5.5 DSB/100 Mbp. Claesson *et al.* [4] reported an initial amount of 35 DSB/100 Mbp from irradiation with ^{211}At (20 Gy). This is further indication that the irradiation performed in the study presented here has failed in some respect.

In summary, we here present a dosimetric model for alpha-particle irradiation from ^{213}Bi. Presented is also an evaluation of complex DSBs following high-LET irradiation experiments and a discussion of expected radiobiological consequences presented in previously published studies.

References

[1] N. Chouin, K. Bernardeau, F. Davodeau, M. Cherel, A. Faivre-Chauvet, M. Bourgeois, C. Apostolidis, A. Morgenstern, A. Lisbona, M. Bardies, Evidence of extranuclear cell sensitivity to alpha-particle radiation using a microdosimetric model. I. Presentation and validation of a microdosimetric model, Radiat Res 171(2009) 657-663.

[2] G. Sgouros, J.C. Roeske, M.R. McDevitt, S. Palm, B.J. Allen, D.R. Fisher, A.B. Brill, H. Song, R.W. Howell, G. Akabani, W.E. Bolch, R.F. Meredith, B.W. Wessels, P.B. Zanzonico, MIRD Pamphlet No. 22 (abridged): radiobiology and dosimetry of alpha-particle emitters for targeted radionuclide therapy, J Nucl Med 51(2010) 311-328.

[3] D.A. Mulford, D.A. Scheinberg, J.G. Jurcic, The promise of targeted {alpha}-particle therapy, J Nucl Med 46 Suppl 1(2005) 199S-204S.

[4] A.K. Claesson, B. Stenerlow, L. Jacobsson, K. Elmroth, Relative biological effectiveness of the alpha-particle emitter (211)At for double-strand break induction in human fibroblasts, Radiat Res 167(2007) 312-318.

[5] H.C. Newman, K.M. Prise, B.D. Michael, The role of higher-order chromatin structure in the yield and distribution of DNA double-strand breaks in cells irradiated with X-rays or alpha-particles, Int J Radiat Biol 76(2000) 1085-1093.

[6] T. Back, L. Jacobsson, The alpha-camera: a quantitative digital autoradiography technique using a charge-coupled device for ex vivo high-resolution bioimaging of alpha-particles, J Nucl Med 51(2010) 1616-1623.

[7] S.Y.F. Chu, L.P. Ekström, R.B. Firestone, WWW Table of Radioactive Isotopes, (1999).

[8] R.A. Boll, D. Malkemus, S. Mirzadeh, Production of actinium-225 for alpha particle mediated radioimmunotherapy, Applied Radiation and Isotopes 62(2005) 667-679.

[9] F.H. Ruddy, A.R. Dulloo, J.G. Seidel, B. Petrovic, Separation of the alpha-emitting radioisotopes actinium-225 and bismuth-213 from thorium-229 using alpha recoil methods, Nuclear Instruments and Methods in Physics Research Section B: Beam Interactions with Materials and Atoms 213(2004) 351-356.

[10] M. Hada, A.G. Georgakilas, Formation of clustered DNA damage after high-LET irradiation: a review, J Radiat Res (Tokyo) 49(2008) 203-210.

[11] K. Magnander, R. Hultborn, K. Claesson, K. Elmroth, Clustered DNA damage in irradiated human diploid fibroblasts: influence of chromatin organization, Radiat Res 173(2010) 272-282.

[12] E. Sage, L. Harrison, Clustered DNA lesion repair in eukaryotes: Relevance to mutagenesis and cell survival, Mutat Res(2010).

[13] E.J. Hall, A.J. Giaccia, Radiobiology for the radiologist, Lippincott Williams & Wilkins, Philadelphia, 2006, ix, 546 p. pp.

[14] H. Olsson, Tumörsjukdomar, 1996.

[15] D.T. Goodhead, The initial physical damage produced by ionizing radiations, Int J Radiat Biol 56(1989) 623-634.

[16] E. Hoglund, E. Blomquist, J. Carlsson, B. Stenerlow, DNA damage induced by radiation of different linear energy transfer: initial fragmentation, Int J Radiat Biol 76(2000) 539-547.

[17] J.C. Roeske, B. Aydogan, M. Bardies, J.L. Humm, Small-scale dosimetry: challenges and future directions, Semin Nucl Med 38(2008) 367-383.

[18] J.C. Roeske, M. Hoggarth, Alpha-particle Monte Carlo simulation for microdosimetric calculations using a commercial spreadsheet, Phys Med Biol 52(2007) 1909-1922.

[19] J.F. Ziegler, PARTICLE INTERACTIONS WITH MATTER, 2011.

[20] M. Ohlson, Optimising a method for visualising γH2AX-foci after irradiation with X-ray and Astatine-211, Department of Radiation Physics, Gothenburg, 2006.

[21] H.H. Rossi, M. Zaider, Microdosimetry and its applications, Springer, New York, 1996, xii, 321 p. pp.

[22] D. Blocher, In CHEF electrophoresis a linear induction of dsb corresponds to a nonlinear fraction of extracted DNA with dose, Int J Radiat Biol 57(1990) 7-12.
[23] S.R. Cherry, J.A. Sorenson, M.E. Phelps, Physics in nuclear medicine, Saunders, Philadelphia, PA, 2003, xiii, 523 p. pp.
[24] ASTAR. Stopping-power and range tables for helium ions, NIST.
[25] M. Lobrich, P.K. Cooper, B. Rydberg, Non-random distribution of DNA double-strand breaks induced by particle irradiation, Int J Radiat Biol 70(1996) 493-503.
[26] H. Hoglund, B. Stenerlow, Induction and rejoining of DNA double-strand breaks in normal human skin fibroblasts after exposure to radiation of different linear energy transfer: possible roles of track structure and chromatin organization, Radiat Res 155(2001) 818-825.
[27] K. Claesson, M. Lyckesvärd, K. Magnander, S. Lindgren, K. Elmroth, Double-Strand Break Repair and Cell Cycle Arrest Activation in Stationary and Cycling Diploid Cells Irradiated with High- and Low-LET Radiation, Radiobiological Effects of Alpha-Particles from Astatine-211, Gothenburg.
[28] K.H. Karlsson, B. Stenerlow, Focus formation of DNA repair proteins in normal and repair-deficient cells irradiated with high-LET ions, Radiat Res 161(2004) 517-527.
[29] H. Wang, X. Wang, P. Zhang, Y. Wang, The Ku-dependent non-homologous end-joining but not other repair pathway is inhibited by high linear energy transfer ionizing radiation, DNA Repair (Amst) 7(2008) 725-733.

Appendix A.1 - Code

Data retrieval

```
%Script for retrieval of data

[filename pathname] = uigetfile('*.xlsx', 'Select file');
addpath(pathname);
[numeric] = xlsread(filename, -1);
```

Dose calculation for irradiation experiment

```
%DOSVol, corrected dosimetric model
clearvars -except numeric
tic;
%Geometry & Distances  [cm]
d = 2.5e-4;          %Nuclear radius
CSDA = 90e-4;        %CSDA-range of alpha particle
th = 8e-4;           %cell layer thickness
deltar = 1e-7;       %Step length of r
deltai = 1e-7;       %Step length for interpolation of stopping-p curve
%Aktivitet
Ac = 1e6;        %Activity conc. [Bq/cm3]
g = 0.9791;
T12 = 45.59;         %Half-life [min]
t1 = 0;              %Start time of irradiation [min]
t2 = 60;             %Stop time of irradiation [min]
%--------------------
mcl = 4*d/3;         %mean chord length of nucleus
if d <= th/2;
   r = th/2:deltar:CSDA+th/2;
else
   r = d:deltar:CSDA+d;
end
lambda = log(2)/T12;
rp = 0:deltai:CSDA+mcl*10;
rm = zeros(1,length(r)-1);         %preallocation of rm
for k = 2:length(r)
   rm(k-1) = (r(k)+r(k-1))/2;      %Distance to the midpoint of each shell
end
%---------------------------------------
%Preallocation to increase computational speed
OHM = zeros(1,length(rm));      %probability of a hit
Si = zeros(1,length(rp));       %Interpolated Stopping power
Sarea = zeros(1,length(rm));    %Energy deposition from individual shell

%---------------------------------------

%calculation of the probability of a hit
OHM = 0.5*(1-cos(asin(d./rm)));  %P(hit)as function of r

%calculation of shell volume
for m = 2:length(r)
Vskal1(m-1) = (pi/3)*((r(m)-th/2)^2)*(3*r(m)-(r(m)-th/2));
Vskal2(m-1) = (pi/3)*((r(m-1)-th/2)^2)*(3*r(m-1)-(r(m-1)-th/2));
Vshell = Vskal1-Vskal2;
```

```
['Calculating shell volume: ' num2str(round(m/length(r)*100)) ' %']
end

%Total number of decays per cm3
Ct = Ac/(log(2)/(T12*60))*g*(exp(-lambda*t1)-exp(-lambda*t2));

%Antal alfa-partiklar som träffar volymen mellan t=t1 & t2
F = Ct*(OHM.*Vshell);

%% Evaluation of the stopping power curve over volume of interest

x = [numeric(:,1)' 0.01];   %radial vector
S = [numeric(:,2)' 0];      %Stopping-power as function of distance (MeV/cm)

Si = interp1(x,S,rp,'cubic');
h = 1;
xdiff = deltai;
%-------------------------------------------------
%Preallocation
r1 = round((rm-d)/deltai+1);
r2 = round((rm-d+mcl)/deltai);
span = r2(1)-r1(1);
xin = zeros(1, span);
Sin = zeros(1, span);
area = zeros(1, span-1);
%-------------------------------------------------
while h <= length(rm);
   xin = rp(r1(h):r2(h));
   Sin = Si(r1(h):r2(h));
   for q = 2:length(xin)
      meanSin = (Sin(q-1)+Sin(q))/2;
      area(q-1) = meanSin*xdiff;
   end
   Sarea(h) = sum(area);
   ['Calculating absorbed dose: ' num2str(round(h/length(rm)*100)) ' %']
   h = h+1;
end
%--------------------------------
tid = toc;
Dos = 1.602e-10*sum(Sarea.*F)/(d^3*4*pi/3)
```

Dosimetric model used for comparison to previously published results

```
%DOSmicro, for comparison to previously published results
clearvars -except numeric
tic;
%Geometry & distances [cm]
d = 8e-4;            %Nuclear radius
CSDA = 85e-4;        %CSDA-range of alpha particle
cyt = 15e-4;         %Cell radius
deltar = 1e-7;       %Step length of r
deltai = 1e-7;       %Step length for interpolation
%-------------------
mcl = 4*d/3;      %Mean chord length
r = cyt:deltar:CSDA+cyt;
```

```
rp = 0:deltai:CSDA+mcl*11;

rm = zeros(1,length(r)-1);         %Preallocation of rm
for k = 2:length(r)
   rm(k-1) = (r(k)+r(k-1))/2;      %distance to midpoint of shell
end
%---------------------------------------
%Preallocation
Vskal = zeros(1,length(rm));    %Shell volume
Si = zeros(1,length(rp));       %interpolated Stopping power
Sarea = zeros(1,length(rm));    %Energy deposition
%---------------------------------------

% Calculation of shell volume
for m = 2:length(r)
theta1 = 0;
theta2 = pi;
Vskal(m-1) = 2*pi/3*(r(m)^3-r(m-1)^3)*(cos(theta1)-cos(theta2));
['Calculating shell volume: ' num2str(round(m/length(r)*100)) ' %']
end

%% Energy deposition

x = [numeric(:,1)' 0.01];   %x-vector
S = [numeric(:,2)' 0];      %Stopping-power as function of distance (MeV/cm)

Si = interp1(x,S,rp,'cubic');
h = 1;
xdiff = deltai;
%-----------------------------------------------
%Preallocation
r1 = round((rm-d)/deltai+1);
r2 = round((rm-d+mcl)/deltai);
span = r2(1)-r1(1);
xin = zeros(1, span);
Sin = zeros(1, span);
area = zeros(1, span-1);
%-----------------------------------------------
while h <= length(rm);
   xin = rp(r1(h):r2(h));
   Sin = Si(r1(h):r2(h));
   for q = 2:length(xin)
      meanSin = (Sin(q-1)+Sin(q))/2;
      area(q-1) = meanSin*xdiff;
   end
   Sarea(h) = sum(area);
   ['Calculating energy deposition: ' num2str(round(h/length(rm)*100)) ' %']
   h = h+1;
end
%------------------------------
Edep = mean(sum(Sarea.*Vskal)/sum(Vskal));
z = 1.602e-10*Edep/(4*pi*d^3/3)     %Mean specific energy
tid = toc;
```

Appendix A.2 – Stopping-Power Tables

8.376 MeV		5.869 MeV	
Distance (cm)	**S (MeV/cm)**	**Distance (cm)**	**S (MeV/cm)**
0.00E+00	634	0.00E+00	821.677
1.00E-04	634.666	5.00E-05	821.677
2.00E-04	637.397	1.00E-04	819.166
3.00E-04	640.291	1.50E-04	821.711
4.00E-04	643.254	2.00E-04	826.848
5.00E-04	646.753	2.50E-04	834.839
6.00E-04	649.002	3.00E-04	834.507
7.00E-04	652.583	3.50E-04	839.347
8.00E-04	655.921	4.00E-04	846.444
9.00E-04	659.266	4.50E-04	851.44
1.00E-03	663.996	5.00E-04	854.844
1.10E-03	667.916	5.50E-04	858.155
1.20E-03	672.645	6.00E-04	862.284
1.30E-03	677.386	6.50E-04	869.877
1.40E-03	681.266	7.00E-04	877.175
1.50E-03	685.181	7.50E-04	878.443
1.60E-03	690.868	8.00E-04	886.437
1.70E-03	695.962	8.50E-04	888.723
1.80E-03	699.361	9.00E-04	891.228
1.90E-03	703.901	9.50E-04	898.629
2.00E-03	710.476	1.00E-03	907.729
2.10E-03	716.218	1.05E-03	910.404
2.20E-03	720.989	1.10E-03	913.466
2.30E-03	726.657	1.15E-03	921.263
2.40E-03	733.28	1.20E-03	929.564
2.50E-03	739.332	1.25E-03	937.921
2.60E-03	744.909	1.30E-03	942.161
2.70E-03	750.242	1.35E-03	953.083
2.80E-03	756.916	1.40E-03	957.431
2.90E-03	763.513	1.45E-03	965.55
3.00E-03	770.958	1.50E-03	966.604
3.10E-03	776.449	1.55E-03	971.812
3.20E-03	782.986	1.60E-03	982.777
3.30E-03	791.299	1.65E-03	989.977
3.40E-03	799.011	1.70E-03	1000.09
3.50E-03	806.693	1.75E-03	1007.26
3.60E-03	813.412	1.80E-03	1013.73
3.70E-03	820.957	1.85E-03	1025.37
3.80E-03	830.757	1.90E-03	1034.63
3.90E-03	841.209	1.95E-03	1037.51
4.00E-03	849.135	2.00E-03	1048.56
4.10E-03	858.36	2.05E-03	1061.09
4.20E-03	869.494	2.10E-03	1066.56
4.30E-03	878.409	2.15E-03	1077.77
4.40E-03	887.464	2.20E-03	1085.92
4.50E-03	899.273	2.25E-03	1098
4.60E-03	909.754	2.30E-03	1108.98
4.70E-03	921.871	2.35E-03	1124.54
4.80E-03	933.134	2.40E-03	1133.43
4.90E-03	946.424	2.45E-03	1144.63
5.00E-03	958.977	2.50E-03	1156.05
5.10E-03	973.465	2.55E-03	1165.29
5.20E-03	987.274	2.60E-03	1181.4

5.30E-03	1002.53	2.65E-03	1203.84
5.40E-03	1019.41	2.70E-03	1212.4
5.50E-03	1036.98	2.75E-03	1228.77
5.60E-03	1056.09	2.80E-03	1241.64
5.70E-03	1072.66	2.85E-03	1259.05
5.80E-03	1093.73	2.90E-03	1271.23
5.90E-03	1115.83	2.95E-03	1292.43
6.00E-03	1137.94	3.00E-03	1310.95
6.10E-03	1162.77	3.05E-03	1329.22
6.20E-03	1187.73	3.10E-03	1348.46
6.30E-03	1215.25	3.15E-03	1365.83
6.40E-03	1245.71	3.20E-03	1388.48
6.50E-03	1279.18	3.25E-03	1412.32
6.60E-03	1312.96	3.30E-03	1438.75
6.70E-03	1350.01	3.35E-03	1463.35
6.80E-03	1391.36	3.40E-03	1489.75
6.90E-03	1436.72	3.45E-03	1515.6
7.00E-03	1486.55	3.50E-03	1545.27
7.10E-03	1540.7	3.55E-03	1577.68
7.20E-03	1600.9	3.60E-03	1611.57
7.30E-03	1669.2	3.65E-03	1651.71
7.40E-03	1746.13	3.70E-03	1689.96
7.50E-03	1832.95	3.75E-03	1730.91
7.60E-03	1932	3.80E-03	1775.38
7.70E-03	2036.96	3.85E-03	1824.92
7.80E-03	2130.3	3.90E-03	1874.05
7.90E-03	2159.3	3.95E-03	1929.69
8.00E-03	2028.33	4.00E-03	1996.53
8.10E-03	1660.98	4.05E-03	2054.99
8.20E-03	1108.03	4.10E-03	2119.13
8.30E-03	504.326	4.15E-03	2182.21
8.40E-03	102.213	4.20E-03	2246.44
8.50E-03	6.13072	4.25E-03	2291.53
8.60E-03	0.119017	4.30E-03	2306.69
8.70E-03	0	4.35E-03	2285.91
		4.40E-03	2181.32
		4.45E-03	2001.13
		4.50E-03	1736.51
		4.55E-03	1414.36
		4.60E-03	1073.36
		4.65E-03	711.124
		4.70E-03	337.595
		4.75E-03	88.5049
		4.80E-03	9.72978
		4.85E-03	0.23885
		4.90E-03	0